Available online at www.sciencedirect.com
SCIENCE DIRECT
ELSEVIER
Icarus 175 (2005) 419–434
ICARUS
www.elsevier.com/locate/icarus

The spin state of 433 Eros and its possible implications

D. Vokrouhlický [a,*], W.F. Bottke [b], D. Nesvorný [b]

[a] *Institute of Astronomy, Charles University, V Holešovičkách 2, CZ-18000 Prague 8, Czech Republic*
[b] *Southwest Research Institute, 1050 Walnut St, Suite 400, Boulder, CO 80302, USA*

Received 10 September 2004; revised 16 November 2004

Available online 3 March 2005

Abstract

In this paper, we show that Asteroid (433) Eros is currently residing in a spin–orbit resonance, with its spin axis undergoing a small-amplitude libration about the Cassini state 2 of the proper mode in the nonsingular orbital element $\sin I/2 \exp(\imath\Omega)$, where I the orbital inclination and Ω the longitude of the node. The period of this libration is $\simeq$53.4 kyr. By excluding these libration wiggles, we find that Eros' pole precesses with the proper orbital plane in inertial space with a period of $\simeq$61.4 kyr. Eros' resonant state forces its obliquity to oscillate with a period of $\simeq$53.4 kyr between $\simeq$76° and $\simeq$89.5°. The observed value of $\simeq$89° places it near the latter extreme of this cycle. We have used these results to probe Eros' past orbit and spin evolution. Our computations suggest that Eros is unlikely to have achieved its current spin state by solar and planetary gravitational perturbations alone. We hypothesize that some dissipative process such as thermal torques (e.g., the so-called YORP effect) may be needed in our model to obtain a more satisfactory match with data. A detailed study of this problem is left for future work.

Keywords: Asteroids, dynamics; Asteroids, rotation; Eros

1. Introduction

The discovery of the Mars-crossing and Earth-approaching Asteroid (433) Eros is considered a landmark in the history of Solar System exploration.[1] Over 100 years ago, Crommelin (1898) wrote about this asteroid: *'The discovery of a new minor planet is hailed as a rule with equanimity, not to say indifference. The number has grown so large, and they are for the most part of so little practical importance in astronomy, that but few observers care to devote themselves to search for them. But the planet DQ, discovered by Herr Witt of the Urania Observatory, Berlin, on August 13 last, aroused from the first exceptional attention. . . . This orbit is of a very sensational character, and quite revolutionizes some of our ideas of the Solar System.'* Studies of Eros' orbital motion have been used over the years to obtain improved values of several astronomical constants including the solar parallax π_0 (e.g., Newcomb, 1898; Hinks, 1904; note that the Eros-derived π_0 value was not superseded until the late 1960's via planetary radar ranging data), the precession constant for the Earth (e.g., Rabe, 1950) and the Earth–Moon mass (e.g., Rabe and Francis, 1967; Lieske, 1968).

Eros was also the first asteroid whose brightness was found to change with time (von Oppolzer, 1901). The variations in Eros' lightcurve were used to deduce its highly elongated shape, which was unlike all previously known

* Corresponding author. Fax: +420-2-2191-2567.
E-mail address: vokrouhl@mbox.cesnet.cz (D. Vokrouhlický).

[1] After its independent discovery by G. Witt and A. Charlois in August 13, 1898, Eros was provisionally designated 1898 DQ (Witt, 1898). The first orbit determination by Berberich (1898) was a great surprise to many, since the body was found to reside on a Mars-crossing orbit with a close approach distance to Earth of only $\simeq$0.15 AU. Following suggestions by Chandler (1898), a systematic search of this body during previous oppositions was performed back to 1893 (e.g., Pickering, 1905), with the earliest recovered astrometric observations recorded on Harvard Observatory plates taken on October 29, 1893.

0019-1035/$ – see front matter
doi:10.1016/j.icarus.2004.11.017

objects of roughly spherical or slightly ellipsoidal shape.[2] Krug and Schrutka-Rechtenstamm (1937), using an ellipsoidal model, estimated Eros' three axes to be 34.6, 19.3, and 16.3 km, surprisingly close to values estimated by NEAR-Shoemaker ($36 \times 15 \times 13$ km; Yeomans et al., 2000; Veverka et al., 2000).

At the advent of the 21st century, Eros' importance was heightened further when it become the target of the NEAR-Shoemaker mission (e.g., Cheng, 2003). This spacecraft, the first ever to orbit and land on an asteroid, provided insights into numerous topics ranging from Eros' collisional history to its internal structure. It also yielded data of unprecedented accuracy on Eros' orbital and rotational state. With the distance between Eros and Earth determined via the radio link to NEAR-Shoemaker and optical astrometry spanning more than a century, Eros' orbit is now the most accurately known among all asteroids. Moreover, NEAR-Shoemaker's laser rangefinder measurements yielded a solution for Eros' rotation state that is more accurate than the one computed via photometry over the past century (e.g., Ďurech, personal communication, 2004): the formal fractional error in the rotation period determination is now $\simeq 6 \times 10^{-9}$, while the pole position was determined to about a half arc-minute of formal error (e.g., Konopliv et al., 2002; Miller et al., 2002). These results also showed that, to a high degree of confidence, Eros rotates about the principal axis of the maximum moment of inertia. No free wobble in Eros' spin vector in the body-fixed frame was found; an upper bound of $\simeq 0.02^\circ$ was found on its amplitude.

Despite this concentrated effort to study Eros over the last 100 years, we find there are still mysteries in Eros' orbital and rotational history that need to be understood. For example, in this paper we show that Eros' rotation axis is in a resonant state, with long-term spin pole librations taking place about the Cassini state 2 corresponding to the proper mode in the orbital frame precession in space. By investigating how Eros' spin vector was captured into this resonant state, we hope to obtain vital clues that will help us constrain this asteroid's enigmatic origin.

We hypothesize that the capture of Eros' spin vector by a resonance may not be a fluke, but instead may have been produced in an analogous way that caused several Koronis family asteroids to end up with parallel spin axes (Slivan, 2002; Slivan et al., 2003; Vokrouhlický et al., 2003). Like Eros, Koronis family members with parallel rotation poles and prograde spins also librate about Cassini state 2 of the forced mode s_6 in the orbital frame precession (Vokrouhlický et al., 2003).[3] In the Koronis family members situation, the resonant spin state of the prograde members was found to be a byproduct of 2–3 Gyr of steady evolution via thermal torques produced by differential heating (e.g., the YORP effect; Rubincam, 2000; Bottke et al., 2003). These results led Vokrouhlický et al. to conclude that, over the last several Gyr, collisions have played a minimal role in the evolution of the Koronis family spin states. Their evolution timescale was also found to be consistent with the estimated age of the Koronis family found via collisional and dynamical studies (Marzari et al., 1995; Greenberg et al., 1996; Bottke et al., 2001; Chapman, 2003). We believe that a thorough analysis of Eros' spin–orbit resonant state may possibly yield comparable information about its evolutionary history.

2. Secular spin–orbit dynamics

In this section, we briefly review various aspects of secular spin–orbit dynamics that are related to our work. The following discussion is based on several pioneering works by Colombo, Peale, Ward and others (see Colombo, 1966; Peale, 1969, 1977; Ward, 1974, 1975, for details).

Consider a body revolving about the Sun with mean motion n that rotates about its spin axis with the angular frequency ω ($\gg n$). The orbit evolves due to planetary perturbations. For main belt asteroids, this produces a steady precession of the node and pericenter so that the nonsingular orbital elements (such as $\xi = \sin I/2 \exp(\imath \Omega)$, where I is the orbital inclination with respect to a reference plane and Ω is the longitude of the ascending node) are well represented by a limited number of Fourier terms. Representation of the same parameters for planet-crossing asteroids like Eros are more complicated, partly because these bodies can undergo close planetary encounters but also because they can interact with the mean motion and secular resonances that crisscross the inner Solar System. Nevertheless, some approximate representation of ξ (in particular) is needed for our analysis and we shall return to this issue below.

For this study, we explore the long-term evolution of a planet-crossing asteroid (e.g., Eros) whose spin axis coincides with the short axis of its inertia tensor (SAM state). This allows us to average out all frequencies that are comparable or faster than n (periods of years and shorter) from the dynamical equations. In particular, torques $\mathbf{T}$ in the Euler equations $d\mathbf{L}/dt = \mathbf{T}$, where $\mathbf{L}$ is the body's rotational angular momentum, are replaced with their rotation- and orbit-averaged values $\bar{\mathbf{T}}$.

We include the solar gravitational torque into our equations of motion (at the quadruple level, which involves J_2; see Bertotti et al., 2003, Chapter 4) as:

$$\mathbf{T}_{\rm gr} = 3n^2 \left(\frac{a}{R}\right)^3 \frac{E}{R^2} (\mathbf{R}\cdot\mathbf{e})(\mathbf{R}\times\mathbf{e}), \tag{1}$$

[2] Curiously, Innes (1931) reported that Eros had axes of 0.7×0.3 arcsec from April 15, 1924 observations when the asteroid was $\simeq 0.41$ AU from Earth. While the long- and short-axis ratio corresponds rather well to Eros' true value, the reported angular extension of Eros' image overestimates its size by about an order of magnitude over previous estimates.

[3] It is irrelevant, for sake of our discussion, that in the Eros case the Cassini state corresponds to the proper rather than forced mode; the latter is stronger for Koronis asteroids that are closer to Jupiter and whose orbital inclination is very small.

where a is the orbital semimajor axis, $\mathbf{R}$ is the heliocentric position vector of the body, $E = C - \frac{1}{2}(A+B)$ and $A \leqslant B \leqslant C$ are moments of inertia along principal axes, and $\mathbf{e}$ is the unitary vector along the angular velocity direction. Note that the SAM assumption allows us to set $\mathbf{L} = C\omega\mathbf{e}$. With $\overline{\mathbf{RR}}/R^5 = (\mathbf{1} - \mathbf{nn})/(a\eta)^3$, where $\mathbf{1}$ is the unitary tensor and $\mathbf{n}$ is the normal to the osculating plane, and $\eta = \sqrt{1-e^2}$, where e is the orbital eccentricity, we have

$$\bar{\mathbf{T}}_{\rm gr} = -\frac{3}{2}\frac{n^2}{\eta^3} E(\mathbf{n}\cdot\mathbf{e})(\mathbf{n}\times\mathbf{e}). \tag{2}$$

The asteroid's spin axis is defined with respect to the moving orbital plane (Eq. (5) below). The inertial torques resulting from the transformation to the moving frame are (e.g., Bertotti et al., 2003, Chapter 7):

$$\bar{\mathbf{T}}_{\rm in} = \frac{d\mathbf{A}}{dt}\cdot\mathbf{A}^T\cdot\mathbf{L}, \tag{3}$$

where

$$\mathbf{A} = \begin{pmatrix} \cos\Omega & \sin\Omega & 0 \\ -\cos I\sin\Omega & \cos I\cos\Omega & \sin I \\ \sin I\sin\Omega & -\sin I\cos\Omega & \cos I \end{pmatrix} \tag{4}$$

is the rotation matrix of the transformation between the inertial system and the system co-moving with the orbital plane (x-axis along the nodal line and z-axis along orbital angular momentum vector). $\mathbf{A}^T$ is the transposed matrix of $\mathbf{A}$.

A convenient parametrization of $\mathbf{e}$ (i.e., the unit vector along the angular velocity direction) found by earlier analyses (e.g., Laskar and Robutel, 1993; Néron de Surgy and Laskar, 1997) is:

$$\mathbf{e} = \begin{bmatrix} \sin\varepsilon\sin(\psi+\Omega) \\ \sin\varepsilon\cos(\psi+\Omega) \\ \cos\varepsilon \end{bmatrix} \tag{5}$$

with ε the obliquity angle and ψ the precession in longitude (as far as its geometric meaning is concerned, see Fig. 1 in Čapek and Vokrouhlický, 2004). These parameters are also referenced in the moving orbital system. Euler equations then imply the following set of equations for the three dynamical quantities characterizing spin state of the body, namely the rotation frequency ω and the two angles (ε, ψ) from (5):

$$\frac{d\omega}{dt} = \frac{\bar{\mathbf{T}}\cdot\mathbf{e}}{C}, \tag{6}$$

$$\frac{d\varepsilon}{dt} = \mathcal{A}\cos\psi - \mathcal{B}\sin\psi - \frac{\bar{\mathbf{T}}\cdot\mathbf{e}_{\perp 1}}{C\omega}, \tag{7}$$

$$\frac{d\psi}{dt} = \alpha\cos\varepsilon - 2\mathcal{C} - \frac{\cos\varepsilon}{\sin\varepsilon}(\mathcal{B}\cos\psi + \mathcal{A}\sin\psi) - \frac{\bar{\mathbf{T}}\cdot\mathbf{e}_{\perp 2}}{C\omega\sin\varepsilon}. \tag{8}$$

Using these equations, the effect of different torques can be readily interpreted:

- The solar gravitational torque (2) is folded into a simple precession term $\alpha\cos\varepsilon$ in (8), where

$$\alpha = \frac{3}{2}\frac{n^2}{\omega}\frac{\Delta}{\eta^3} \tag{9}$$

and

$$\Delta = \frac{C - \frac{1}{2}(A+B)}{C} \tag{10}$$

is a measure of the body's ellipticity. For Eros, $\Delta = 0.40341$ (e.g., Miller et al., 2002; Konopliv et al., 2002), one of the largest values among the known Solar System bodies (e.g., Vokrouhlický and Čapek, 2002, Fig. 2). Note as well that α changes as a and e change (through n and η, respectively). Using the current Eros' orbital parameters and rotation period (5.27025547 h), we obtain $\alpha \simeq 164.93''/\text{yr}$.
- The inertial terms contain:

$$\mathcal{A} = \cos\Omega\,\dot{I} - \sin I\sin\Omega\,\dot{\Omega}, \tag{11}$$

$$\mathcal{B} = \sin\Omega\,\dot{I} + \sin I\cos\Omega\,\dot{\Omega}, \tag{12}$$

$$\mathcal{C} = \sin^2 I/2\dot{\Omega}, \tag{13}$$

with the dots denoting d/dt. Using a complex notation $\xi = \sin I/2\exp(\imath\Omega)$ we may also write:

$$\mathcal{A} + \imath\mathcal{B} = \frac{2}{\sqrt{1-\xi\bar{\xi}}}\left(\frac{d\xi}{dt} - \imath\xi\mathcal{C}\right), \tag{14}$$

$$\mathcal{C} = \frac{1}{2\imath}\left(\bar{\xi}\frac{d\xi}{dt} - \xi\frac{d\bar{\xi}}{dt}\right) \tag{15}$$

(where $\bar{\xi}$ means the complex conjugate of ξ).
- Additional torques included in $\bar{\mathbf{T}}$, such as internal tides or the YORP effect (Rubincam, 2000), could be derived from the last terms of Eqs. (6)–(8), where we used projection unitary vectors:

$$\mathbf{e}_{\perp 1} = \frac{\mathbf{n} - (\mathbf{n}\cdot\mathbf{e})\mathbf{e}}{\sin\varepsilon}, \tag{16}$$

$$\mathbf{e}_{\perp 2} = \frac{\mathbf{n}\times\mathbf{e}}{\sin\varepsilon}. \tag{17}$$

Except for some discussion of their effects in Section 5, they will not enter into our analysis at this time. Similarly, we also exclude from our spin state analysis gravitational torques produced during planetary close encounters (e.g., Richardson et al., 1998; Scheeres et al., 2000).

When $\bar{\mathbf{T}} = 0$, the angular frequency ω is conserved and variations of ε and ψ may be represented using a one-dimensional Hamiltonian (e.g., Laskar and Robutel, 1993):

$$\mathcal{H}(X,\psi;t) = \frac{\alpha}{2}X^2 - 2\mathcal{C}X + \sqrt{1-X^2}(\mathcal{A}\sin\psi + \mathcal{B}\cos\psi), \tag{18}$$

where $X = \cos\varepsilon$ is a conjugate momentum to ψ. A convenience is that the problem might be analyzed using standard

tools of Hamiltonian mechanics. Despite our simplifications, however, the solution remains nontrivial because of the time dependence of parameters $(\mathcal{A}, \mathcal{B}, \mathcal{C}; \alpha)$. We discuss this case in the next section.

In order to remove the $\sin\varepsilon \simeq 0$ singularity from Eqs. (6)–(8) we set $\zeta_\pm = (1 \pm \cos\varepsilon)\exp(\imath\psi)$ in our integrations. The sign plus is used to remove the singularity near $\varepsilon \simeq 180°$, and thus ζ_+ is used when $\varepsilon > 90°$; the sign minus is used to remove the singularity near $\varepsilon \simeq 0°$, so that ζ_- is used when $\varepsilon < 90°$.

2.1. Cassini states and resonance

In this section, we take advantage of the approximations described above to analytically explore whether Eros is in a spin–orbit resonance. Note that in Eros' present orbital state, $\xi = \sin I/2\exp(\imath\Omega)$ is dominated by a single Fourier term. For $\bar{\mathbf{T}} \sim 0$, $\omega =$ constant, and the system becomes integrable as recalled below.

To start, we assume $\xi = A\exp(\imath\Phi)$ with $\Phi = \sigma t + \phi$. This allows $\mathcal{A} + \imath\mathcal{B}$ to become simple harmonic functions of time $(2A\sqrt{1-A^2}\sigma\exp[\imath(\Phi + \pi/2)] = \sigma\sin I_r\exp[\imath(\Phi + \pi/2)])$ with $\mathcal{C}$ constant. If the orbital eccentricity and the semimajor axis are constant, or they change very little, α is also constant. Note that for Eros, $\sigma \simeq -21.1''/\text{yr}$, $A \simeq 0.1028$ corresponds to the proper inclination of $I_r = 2\text{asin}(A) \simeq 11.8°$ and the phase $\phi \simeq 322°$ is very close to the current osculating longitude of node $\Omega \simeq 304°$ (i.e., these values are given for $t = 0$ at J2000.0).

We now define new canonical variables $X' = -X = -\cos\varepsilon$ and $\varphi = -(\psi + \Phi)$ via a contact transformation generated by $F(\psi, X'; t) = -X'(\psi + \Phi)$. The new Hamiltonian reads[4] $\mathcal{H}' = \mathcal{H} - \sigma X'$, or

$$\mathcal{H}'(X', \varphi) = \frac{\alpha}{2}X'^2 - \sigma\cos I_r X' + \sigma\sqrt{1-X'^2}\sin I_r\cos\varphi. \tag{19}$$

The new equations in mixed variables ε (obliquity) and φ are:

$$\frac{d\varepsilon}{dt} = \sigma\sin I_r\sin\varphi, \tag{20}$$

$$\frac{d\varphi}{dt} = -\alpha\cos\varepsilon - \sigma\cos I_r + \sigma\frac{\cos\varepsilon}{\sin\varepsilon}\sin I_r\cos\varphi. \tag{21}$$

Because the Hamiltonian (19) is time-independent, it is an integral of motion. When rewritten in mixed variables, and scaled by σ, Eq. (19) becomes (compare with Eq. (14) in Colombo, 1966):

$$C(\varepsilon, \varphi) = \kappa\cos^2\varepsilon + \cos I_r\cos\varepsilon + \sin I_r\sin\varepsilon\cos\varphi = \text{const}. \tag{22}$$

Here $\kappa = \alpha/(2\sigma)$, which is the fundamental parameter of the problem.

[4] Recall $d\Phi/dt = \sigma$; for a similar derivation see Ward (1975).

The stationary points in the system described by (20)–(21) are called *Cassini states*. Eq. (20) constrains the stationary values to occur at $\varphi = 0°$ or $\varphi = 180°$, while Eq. (21) yields the value of stationary obliquity from the transcendental equation

$$\kappa\sin 2\varepsilon = -\sin(\varepsilon \pm I_r). \tag{23}$$

Here the upper sign on the right-hand side corresponds to $\varphi = 180°$ and the lower sign corresponds to $\varphi = 0°$. Depending on the value of κ, there are two to four solutions for this equation. In particular, for small values of κ (and $I_r \neq 0$), four Cassini states exist: two of them near the poles of the orbit (the so-called Cassini states 1 and 3, both with $\varphi = 180°$), and two at the intermediate values of obliquity (the so-called Cassini states 2 at $\varphi = 0°$ and 4 at $\varphi = 180°$). The limiting value of $\kappa = \kappa_\star$, for which the Cassini states 1 and 4 bifurcate, depends on the inclination I_r (see, e.g., Henrard and Murigande, 1987):

$$\kappa_\star = -\frac{1}{2}\left(\sin^{2/3} I_r + \cos^{2/3} I_r\right)^{3/2}; \tag{24}$$

$\kappa_\star$ is in between -0.5 and -1, so that for $\kappa < -1$ the four Cassini states exist for any inclination value. We also note that in the limit $I_r \to 0°$, the Cassini states 1 and 4 disappear; this is also readily seen from the first integral (22) whose dependence on φ disappears in this limit. In other words, small inclination states cause the width of the secular spin–orbit resonances to shrink. The resonance zone also shrinks when $\kappa \to -\infty$, which occurs when the obliquities of Cassini states 2 and 4 approach 90°.

Cassini states 2 and 4, which are stable and unstable points of a resonance zone enclosed by a separatrix, are directly relevant to our work on Eros' spin state. In Eros' case, we have a value of κ ($\simeq -3.603$, with $\sigma \simeq -21.1''/\text{yr}$) that guarantees the existence of the resonance zone and all four Cassini states. Inserting the relevant values into Eq. (23), we find that $\varepsilon_\star \simeq 82.35°$ for the obliquity of the Cassini state 2, fairly close to Eros' obliquity of $\simeq 89°$ (e.g., Miller et al., 2002; Souchay et al., 2003). This hints that Eros may currently be residing in a spin–orbit resonance.

To further explore the suggestion that Eros may be librating about Cassini state 2 of the proper mode in ξ, we estimated the maximum width of the resonance zone about Cassini state 2 from Colombo's integral (22). We find that for $\varphi = 0°$, the resonance zone stretches from $\simeq 63°$ to $\simeq 100°$, thus comfortably enclosing the Eros value (Fig. 1). Further confirmation will require more complicated tests involving the value of φ and ξ and a direct numerical integration.

A linearized analysis of small oscillations about the Cassini state 2 yields a frequency:

$$\sigma_{\text{lib}} = \sigma\sqrt{D\sin I_r}, \tag{25}$$

with

$$D = \cos I_r\frac{\sin\varepsilon_\star}{\cos\varepsilon_\star} + \sin I_r\left(\frac{\cos\varepsilon_\star}{\sin\varepsilon_\star}\right)^2, \tag{26}$$

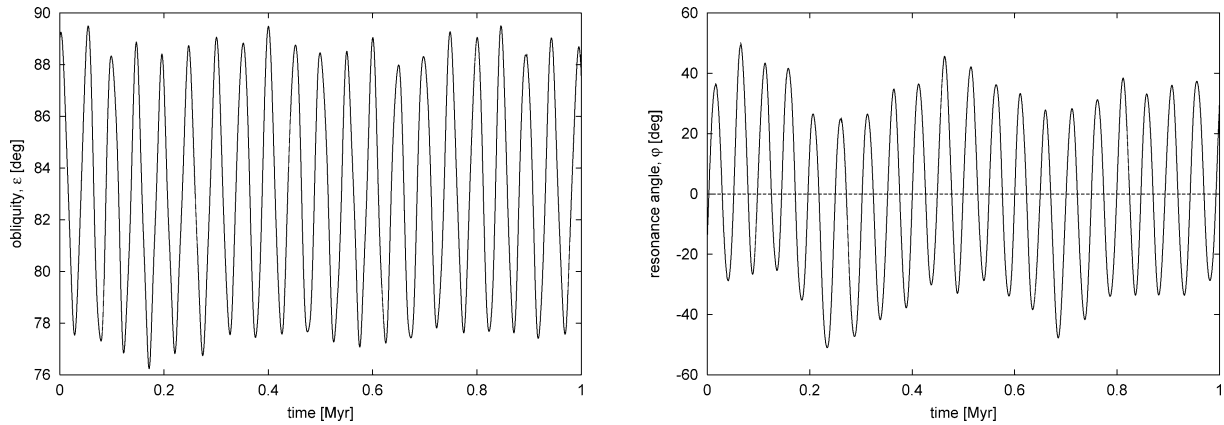

Fig. 1. (Left part) Variations of Eros' obliquity during the next Myr (time origin is J2000.0; compare with Fig. 5 in Skoglöv, 1997). We use the nominal Eros' orbit—see also Fig. 2—and initial spin data from Miller et al. (2002). Note that the large oscillations of the obliquity indicate the presence of secular resonance. (Right part) Critical angle $\varphi = -(\psi + \Phi)$ defined for the phase Φ of the dominant (proper) term in ξ. Small amplitude librations indicate that Eros' pole is locked near the Cassini state 2.

where $\varepsilon_\star$ is a solution of (23). Inserting known values for Eros into (25), we estimate that Eros' pole would librate with a period $\simeq$50.3 kyr.

3. Eros' spin–orbit resonance

With the insights gleaned from our analytical estimates, we are now ready to investigate Eros' rotation state using numerical integration. Because Eros' rotational history is connected to its orbital history, we need to obtain some knowledge of Eros' orbital evolution history before proceeding. This is a problem because most near-Earth asteroids (NEA) orbital histories are highly chaotic, with numerous encounters with planets and multiple interactions with secular and mean motion resonances (Milani et al., 1989; Froeschlé et al., 1995; Michel and Thomas, 1996; Michel and Froeschlé, 1997; Michel, 1997; Michel et al., 1998). This means that it is impossible to track the true orbital paths followed by NEAs more than a few hundred years into the past or future.

An approximate method that can be used to gain information about Eros' future orbital history is to numerically integrate Eros' orbit (and that of numerous clones, as we will discuss below) forward in time (e.g., Michel et al., 1998). The broad evolution patterns represented by these orbital histories can be used to help us characterize the likely fate of Eros. (A discussion of Eros' previous orbital and spin history is in the next section.) Using Eros' current ephemeris obtained in the `AstOrb` file (ftp://ftp.lowell.edu), we tracked its orbit backwards and forwards in time for 0.1 and 1 Myr, respectively, using the code `swift-rmvs3` (Levison and Duncan, 1994). Next, we numerically integrated the system of equations given by (6)–(8) with $\bar{\mathbf{T}} = 0$ and $(\mathcal{A}, \mathcal{B}, \mathcal{C}; \alpha)$ determined from our orbital integration data. The effects of planetary close encounters and YORP were ignored, thus the rotation frequency ω was kept constant. Our initial values for obliquity ε and the precession in longitude ψ were $\varepsilon_0 = 89.01°$ and $\psi_0 = 72.42°$, respectively (Miller et al., 2002; Souchay et al., 2003). Note that our results will not be as accurate as Souchay et al. (2003), who included all short-periodic effects and the possible free motion of Eros' rotation pole in the body, but they do correctly represent the long-term evolution of the pole parameters.

Figure 1 (left panel) shows Eros' obliquity oscillating between $\simeq$76° and $\simeq$89.5° with a dominant period of $\simeq$53.4 kyr. These values coincide with our derived value for small oscillations about Cassini state 2 (Section 2), with the period slightly increased because of a nonzero libration amplitude. Note that this behavior was first seen by Skoglöv (1997), though he did not dwell on his discovery (e.g., Souchay et al., 2003).

To confirm that Eros' spin resides near Cassini state 2, we need to define and examine the libration of the resonant angle φ (Section 2). To do so, we need to define the Fourier term that can represent the nonsingular orbital element ξ and compute its phase Φ. As mentioned previously, any Fourier representation of ξ over large time intervals may be invalid if Eros experiences a close planetary encounter or if it interacts with a resonance. For short timespans (0.01–0.1 Myr), however, Eros' orbital elements may be stable enough that "proper elements" can be defined using methods similar to those described by Gronchi and Milani (2001).

In our approach we consider a running window of 0.2 Myr for which a spectral density S_ξ of ξ is computed using a technique by Ferraz-Mello (1981). We then find a maximum for S_ξ over this interval that corresponds to the statistically best Fourier-like representation of ξ. The amplitude A, frequency σ and phase ϕ of this term are then computed, with all three parameters used to define the proper orbital inclination I_r and the resonant angle $\varphi = -(\psi + \Phi)$. The phase ϕ is Φ in the middle epoch of the running window. Using this method with Eros' J2000.0 osculating orbital elements, we obtain values similar to the proper elements found at the `NeoDyS` page (http://newton.dm.unipi.it/) (and Section 2.1).

Figure 1 (right panel) shows the behavior of φ for the next Myr along Eros' nominal orbit. The observed small-amplitude librations about 0° indicate that Eros' spin pole is librating about Cassini state 2 of the proper mode in the ξ representation. (Traditionally, the corresponding frequency of the proper mode is denoted s $(=\sigma)$ (e.g., Morbidelli, 2002); we shall thus speak about the (secular) spin–orbit or s-resonance.) Hence, in inertial space, Eros' pole follows the $\simeq$61.4 kyr proper motion of its orbital frame (with some small oscillations about that value). Our result thus suggests that the long precession frequency of $\simeq$450 kyr postulated by Souchay et al. (2003) never occurs.

3.1. Capture and stability of Eros' spin pole in the s-resonance

Here we investigate the likelihood that Eros' pole will remain trapped in the s-resonance into the future as Eros' orbit and pole parameters undergo evolution. Our method was to numerically integrate Eros' nominal orbit and 9 clones (with their initial orbital conditions inside their current uncertainty interval)[5] for 25 Myr into the future using `swift-rmvs3`. We also integrated backwards for 0.1 Myr to help us define proper elements for our test bodies. Note that the orbits of planet-crossing asteroids are chaotic enough that any single numerical representation probably does not represent Eros' long-term future evolution. Still, some of our clones may adhere closely to it (especially during short integration intervals).

We found that the orbits of our test bodies diverged on a $\simeq$0.1 Myr timescale, with only 3 clones thrown out of the inner Solar System before 25 Myr had elapsed. This confirms an unusually long dynamical lifetime of Eros' orbit, compatible with an estimate of $\simeq$50 Myr by Michel et al. (1998). We used these evolution tracks as input to numerically integrate Eqs. (7)–(8). Eros' current rotation state was included in our model as an initial condition, while we assumed $\bar{\mathbf{T}} = 0$ (which makes ω constant). Our orbital and spin evolution results for three representative cases are discussed below.

3.1.1. Test case #1: Interaction with one or more spin orbit resonances

Figure 2 shows how Eros' current osculating orbital elements, what we call its nominal orbit, evolves into the future. Our results show the following trends. For the first 20 Myr of our simulation, Eros' semimajor axis a bounces between the 5/9 and 4/7 mean motion resonances with Earth. Its orbital eccentricity e stays between 0.15 and 0.35 over 25 Myr, which tends to keep it away from close Earth encounters. It only achieves an Earth-crossing orbit for short intervals near 10 and 16 Myr. Eros' orbital inclination I undergoes an interesting large and long-period variation for 5–10 Myr as a result of the ν_{14} secular orbital resonance, which is characterized by $s \simeq s_4 \simeq -17.75''/\text{yr}$. Nevertheless, the evolution of Eros' osculating inclination over 25 Myr is reasonably well characterized by the proper inclination I_r computed using the method in Section 3. This match suggests that the proper term dominates contribution in ξ over our integration time. Finally, we see that the variations in proper frequency s are related to our a and I changes.

Figure 3 shows the evolution of the obliquity ε and the critical angle φ of the s-resonance integrated along our nominal Eros orbit. At $\simeq$8 Myr, the spin state escapes the resonance and only regains it again for a brief period near $\simeq$15 Myr (but with much larger libration amplitude). The increase of libration amplitude produced for >7 Myr is caused by Eros' interaction with the ν_{14} secular resonance, when its proper frequency s is close to the planetary (forced) frequency s_4. (Note that the ν_{13} resonance associated with $s \simeq s_3 \simeq -18.85''/\text{yr}$ has a smaller effect.) As explained in the previous section, Eros' spin pole evolution follows the reference frame tied to the s mode in ξ until the contribution from s_4 in ξ becomes important. The Fourier analysis of ξ shows that ξ for 5 Myr $< t <$ 9 Myr can be represented by two terms: the proper term with 18°–25° amplitude and $\simeq -20''/\text{yr}$ frequency and a term with $\simeq$1° amplitude and $\simeq -40''/\text{yr}$ frequency. This second high-frequency term does not exist for $t <$ 5 Myr. For $t >$ 5 Myr, the proper and the high-frequency terms interact and produce large-scale chaos observed in Eros' spin evolution. We demonstrate this by studying the dynamics of (7) and (8) with two Fourier terms included in $\mathcal{A}$, $\mathcal{B}$, and $\mathcal{C}$. We find that the libration islands corresponding to the two Fourier terms in ξ for $t >$ 5 Myr are comparable in size and overlap. Hence, the spin vector is chaotically driven out of the s-resonance and exits the resonant state at $\simeq$8 Myr.

3.1.2. Test case #2: How planetary encounters might effect Eros

Figure 4 shows future orbital evolution of our first Eros clone. In this case, a slowly drifts inward while interacting with various mean motion resonances. After 10.3 Myr, a close Earth encounter moves it slightly inside 1 AU. It keeps this value until $\simeq$23.5 Myr, when a second Earth encounter moves it out of the inner Solar System and into the 2/1 mean motion resonance with Jupiter, where it remains for a short time until falling into the Sun. The clone's e and I values undergo several long-period variations, an indication of secular orbital resonances at work (e.g., ν_{13}, ν_{14}), until the close Earth encounter $\simeq$23.5 Myr. These resonant captures do not affect the mean osculating value of I enough to affect our estimate for proper I_r, but they do keep the proper frequency s moderately high for the length of our integration.

Figure 5 shows the evolution of this clone's spin state parameters. Though the obliquity is observed to jump in and out of the s-resonance several times during the integration, we focus here on what happens during the close Earth en-

[5] In particular, we displace the initial X coordinate of nominal Eros orbit by multiples of 10^{-12} AU.

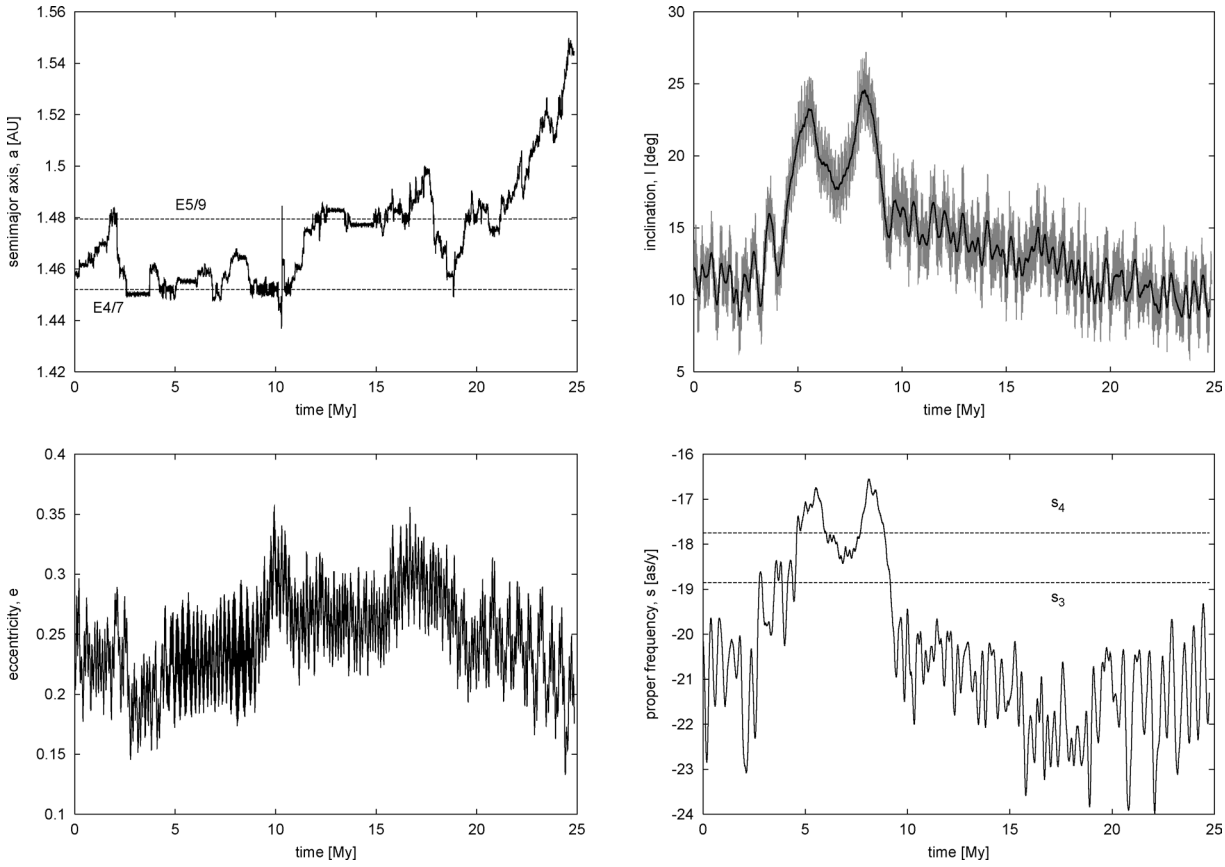

Fig. 2. Evolution of the nominal Eros' orbit for the next 25 Myr: semimajor axis (left and top), eccentricity (left and bottom), inclination (right and top), and dominating (proper) frequency in ξ (right and bottom). Interesting features include: (i) the orbit does not undergo any substantial close encounters with the terrestrial planets but it bounces between various mean-motion and secular resonances in the planet-crossing region (the dashed lines in the upper left panel indicate the exterior $5/9$ and $4/7$ resonances with the Earth); (ii) the osculating value of the inclination (gray curve in the upper right panel) is well represented by the dominant (proper) Fourier term in $\xi = \sin I/2 \exp(\imath\Omega)$ (the thick black curve) defined by the procedure in the text; (iii) the inclination undergoes large and long-period oscillations when interacting with secular resonances ν_{13} and ν_{14}, whose frequencies $s_4 \simeq -17.75''/\mathrm{yr}$ and $s_3 \simeq -18.85''/\mathrm{yr}$ are shown in the bottom right panel by the dashed lines.

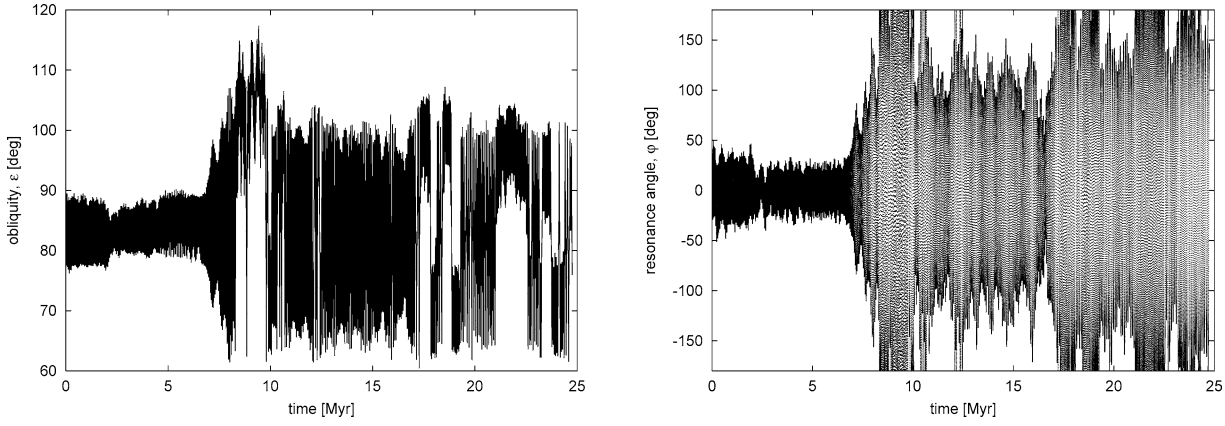

Fig. 3. Evolution of Eros' obliquity ε (left part) and the critical angle φ of the spin–orbit s-resonance (right part) integrated along the nominal orbit from Fig. 2. Our model asteroid departs the spin–orbit resonant state at $\simeq$8 Myr due to overlapping modes s and s_4 in ξ.

counter occurring at $\simeq$10.3 Myr. As observed in Fig. 4, a and e both undergo dramatic changes that decrease α and κ and shrink the width of the resonance zone about Cassini state 2 (Section 2.1). A zoom of the event is shown in Fig. 6. We see that the previously-librating critical angle φ is pushed to a separatrix, which it adheres to for the remainder of the plotted evolution time. The spin–orbit resonant state is eventually regained but only for a short time; with Eros' interaction with the ν_{14} resonance the source of the pole's instability.

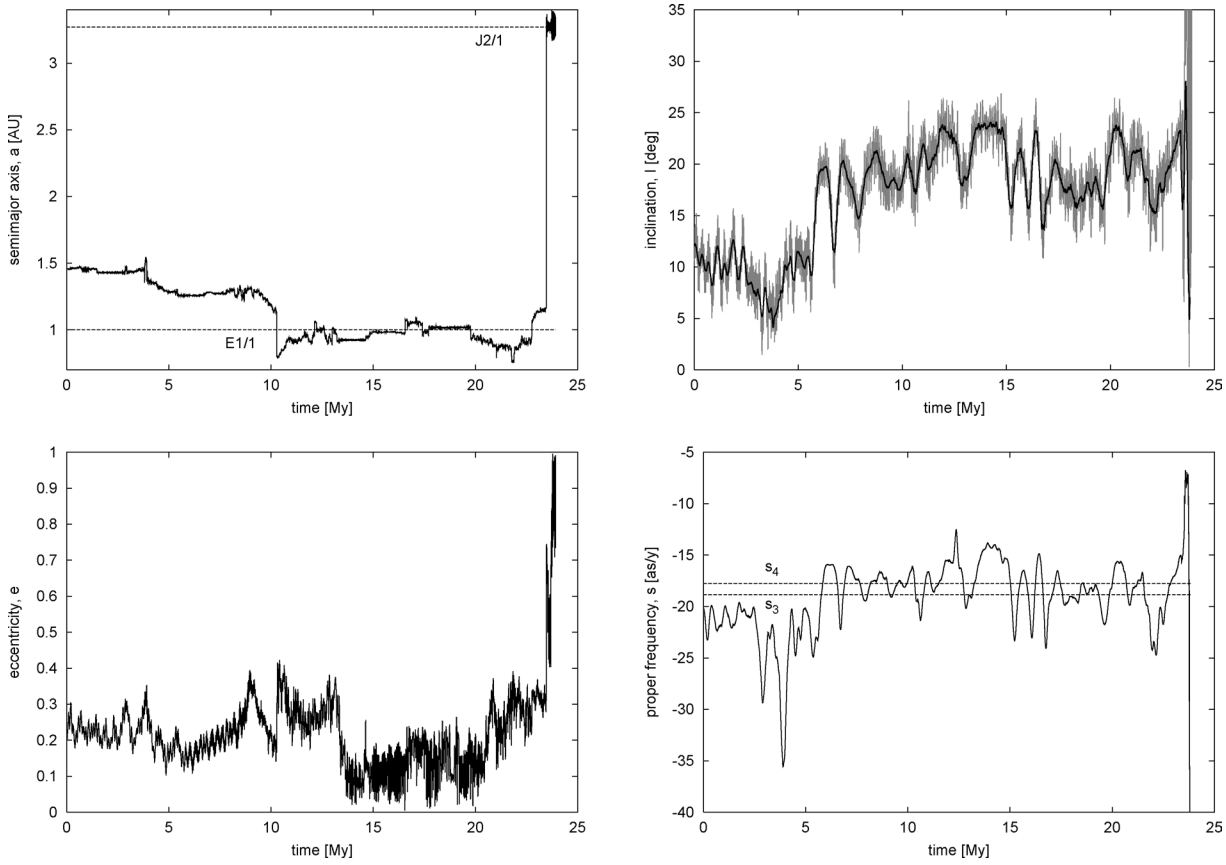

Fig. 4. The same as in Fig. 2 but for the Eros clone described in test case #2. The model asteroid is brought near Earth, where it resides temporarily locked in various exterior and interior mean-motion resonances with Earth (including the co-orbital state; dashed lines in the upper left panel indicate the Earth co-orbital resonance E1/1 and the 2/1 mean motion resonance with Jupiter).

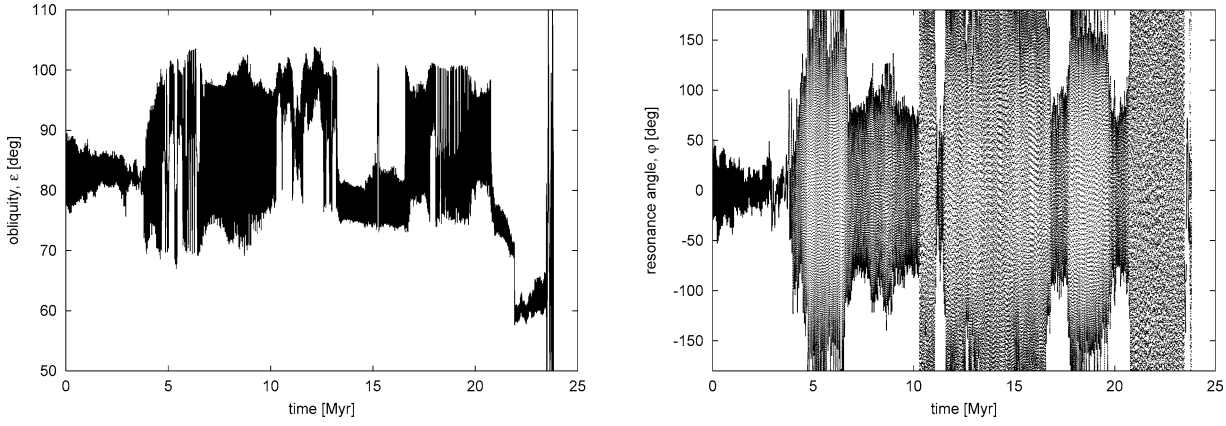

Fig. 5. Evolution of Eros' obliquity ε (left part) and the critical angle φ of the s spin–orbit resonance (right part) integrated along the orbit from Fig. 4. Librations are intermixed with circulations as a response to various perturbations such as a close encounter with Earth (Fig. 6).

3.1.3. Test case #3: The effect of a steady drop in inclination

Figure 7 shows the future orbital evolution of a different Eros clone. We see that its orbit is decoupled from the Earth influence until a close Earth encounter at $\simeq$11.5 Myr. After that, numerous planetary encounters eventually push a to $\simeq$2.1 AU, where the ν_6 resonance sends the asteroid into the Sun. For e, we see a steady increases between 11–13.5 Myr until it is interrupted by a second close Earth encounter, and from there we see it go to 1 via the ν_6 resonance. The cyclic variations in I are produced by the ν_{14} resonance. The feature at $\simeq$4.5 Myr is caused by interactions with the ν_3 resonance, which also happens to weakly affect e. For 11–13.5 Myr, I drops to near zero as e increases.

The most peculiar feature in this clone's orbital evolution can be seen between 11–13.5 Myr where secular resonances

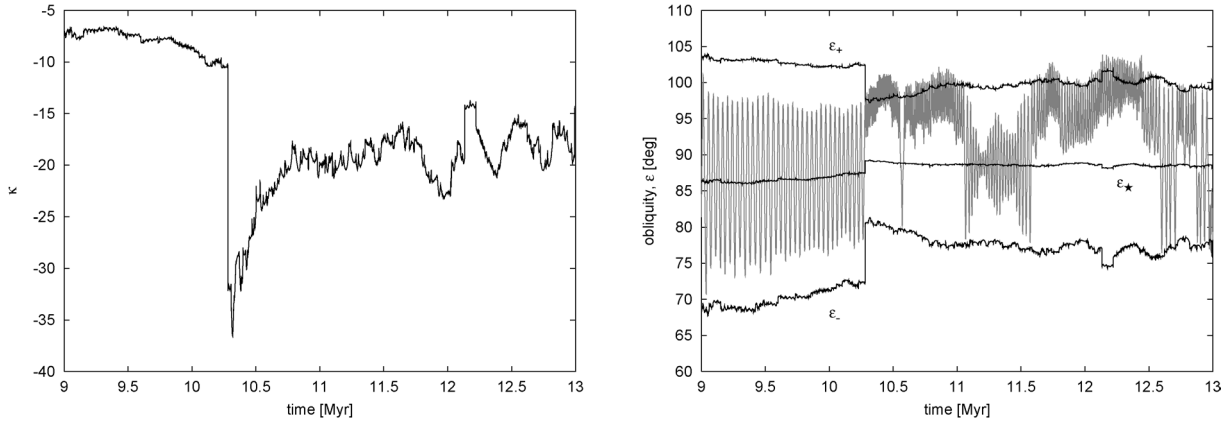

Fig. 6. Results for the Eros clone shown in Fig. 4 (test case #2): (left plot) $\kappa = \alpha/(2\sigma)$, and (right plot) s-resonance zone about Cassini state 2 is shown by its maximum width at $\varphi = 0^\circ$ (solid line ε_+ and ε_-) and the stable point location (solid lines $\varepsilon_\star$). The integrated evolution of the obliquity is superimposed in the right plot using the light solid line. The time interval (abscissa) is near a deep close encounter with the Earth (at $\simeq$10.3 Myr) that triggers an instability of the spin resonant state by crossing the separatrix.

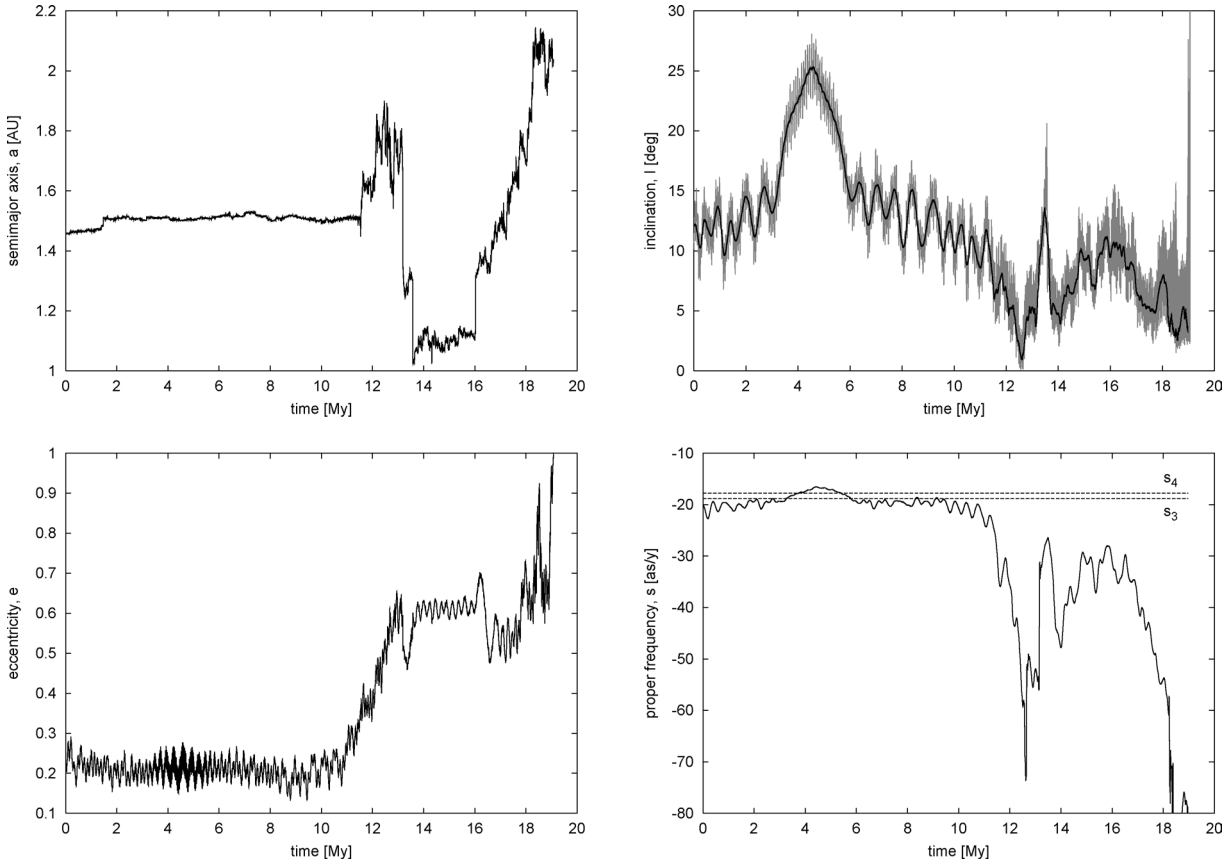

Fig. 7. The same as in Fig. 2 but for the Eros clone described in test case #3. The inclination undergoes a cycle of the ν_{14} resonance at $\simeq$4.5 Myr. The most "perplexing" orbital feature is the steady increase of the model asteroid's orbital eccentricity (and the correlated drop in its inclination) at 11–13.5 Myr.

are at work. The correlated effect on e and I suggests a Kozai-like phenomenon, though the ordinary Kozai does not occur here. Note that the Kozai resonance occurs when the proper orbital frequency s is equal to the proper orbital frequency g of the eccentricity vector $\zeta = e\exp(i\varpi)$, where e is the eccentricity and ϖ the longitude of pericenter (e.g., Morbidelli, 2002).

The pole-parameters evolution for this orbit is shown in Fig. 8. The interaction of the s and s_4 resonances at $\simeq$4.5 Myr triggers an increase in the libration amplitude of φ and the clone's obliquity. There is also an underlying, longer-period, trend produced by the proximity of the s_4 and s_3 resonances. The major perturbation on the stability of the pole in the spin–orbit resonance, however, is caused by I be-

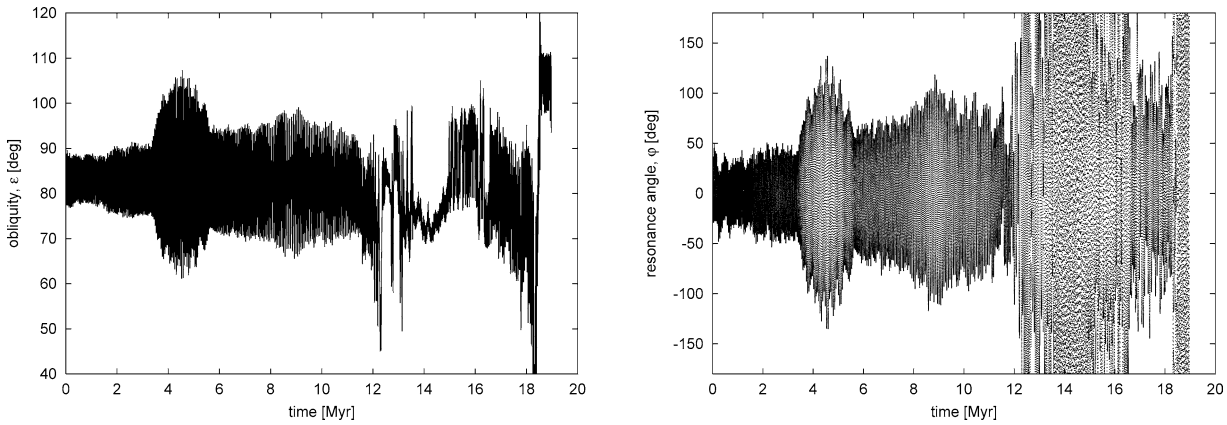

Fig. 8. Variations of Eros' obliquity (left plot) and the critical angle φ of the s spin–orbit resonance (right plot) integrated along the orbit shown in Fig. 7. Interaction of the s and s_4 inclination modes produces a perturbation at $\simeq$4.5 Myr. The model asteroid does not leave the spin–orbit resonance, however, until the inclination becomes too small to keep the libration zone macroscopic at $\simeq$12.5 Myr.

ing driven to small values. As discussed in Section 2.1, when $I_r \to 0°$, the resonance zone about the Cassini state shrinks. If I evolves too quickly compared to the libration period, the process is not adiabatic, the libration amplitude increases up to the separatrix limit, and the pole jumps out of the resonance.

3.1.4. Summary

Using our results, we can draw some conclusions about the dynamics of spin–orbit resonances for Eros, and perhaps for planet-crossing asteroids in general. First, orbital evolution of a, e, I can influence the evolution of the spin axis, with resonant states gained or lost via three main mechanisms:

- Interaction with spin–orbit resonances such as $s \simeq s_4$ (Fig. 3);
- Close planetary encounters that cause changes to a and e (and α and κ) (Fig. 6); and
- Higher-order or Kozai-like secular resonances that can drive I to small values (Fig. 8).

The latter two processes make the spin–orbit resonance about the Cassini state to shrink or disappear.

The median time for our test asteroids to leave the spin–orbit resonance was ∼12 Myr, with 2 clones remaining trapped in the s-resonance for the entire 25 Myr of our integration. Because these bodies were generally decoupled from Earth's influence, it implies that the current position of Eros' pole in the s-resonance may not be a fluke. We investigate this possibility further in the next section.

4. Can Eros' spin state tell us about its past evolution?

In this section, we explore whether Eros' current spin state can constrain its past orbit and spin evolution. Our goal is to determine whether particular main belt regions are more likely to have produced Eros' current state than other regions.

4.1. Eros' orbital evolution

Eros' orbital evolution history can be divided into two phases: (i) its evolution from inside the main belt to a resonance capable of pushing it onto a planet-crossing orbit, which may have taken several Gyr (Chapman et al., 2002; Chapman, 2003), and (ii) its evolution from this resonance to its observed orbit, which may be a short as a few Myr or as long as several tens of Myr (Bottke, 2001). Our simulations in this paper focus solely on the latter phase.

Because NEA orbits are chaotic on 0.1–1 kyr timescales, we cannot integrate Eros backwards in time to determine where it originated. Instead, we assume that Eros' current osculating orbit is one that some asteroids evolving out of the main belt may pass through as they evolve throughout the inner Solar System. If true, we can explore the orbital evolution of Eros in a statistical sense by checking whether the orbital histories of test bodies evolving out of the main belt even pass through Eros' current (a, e, I) orbit. As an analogy, think of the inner Solar System as a pachinko game with Eros' current orbit as one of the special holes that balls find from time to time. Like our test bodies, the trajectory that each ball follows is chaotic and different from all the others. If you play enough balls, however, it is possible that statistical trends may be found in the pathways followed by the balls that enter the special hole.

To this end, we have numerically integrated thousands of test bodies out of the main belt using the techniques described in Bottke et al. (2000, 2002). The starting location for our test bodies were powerful resonances (i.e., ν_6 secular resonance, the 3/1 mean motion resonances with Jupiter) and diffusive regions fed by hundreds of thin resonances located inside the main belt (e.g., the population of asteroids on solely Mars-crossing orbits adjacent to the main belt). These particles were tracked until they collided with the Sun, were thrown beyond 10 AU from the Sun

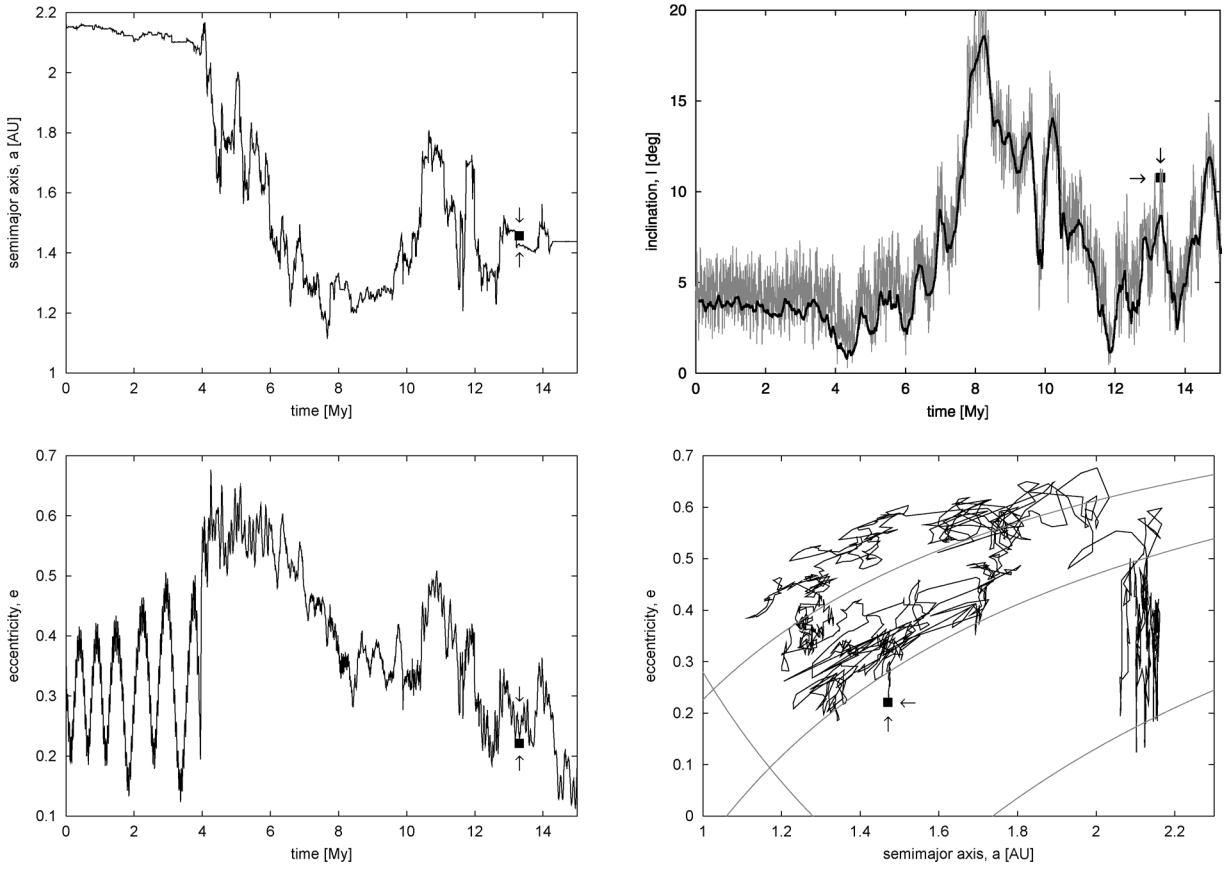

Fig. 9. A possible evolutionary path for Eros if it started in the immediate Mars-crossing region: semimajor axis a (left and top), eccentricity e (left and bottom), inclination I (right and top), and projection onto the a vs. e plane (right and bottom). At $t \simeq 13.18$ Myr, the orbit closely matches the current orbit of Eros shown by the black square (and pointed out by the arrows). Its initial residence in the ν_6 resonance (time $\leqslant$4.5 Myr) make its eccentricity large enough to allow Mars- and later Earth-encounters to drive the orbit more deeply into the planet-crossing region. The gray solid line in the inclination plot shows the osculating value, while the thick solid line is the proper inclination computed by the method outlined in Section 3. The large variation of the inclination near $\simeq$8 Myr is due to the ν_{13} secular resonance (see also the proper s value in Fig. 10). Grey lines in the a vs. e plot are the parameters needed for the model asteroids to reach planet-crossing orbits. Our model asteroid visits both the Mars- and Earth-crossing zones before reaching Eros' current orbit (solid square).

(usually by a close encounter with Jupiter) or they collided with a planet. Our goal was to determine, for each test body trajectory, whether their (a, e, I) parameters came within $\Delta a = 0.02$ AU, $\Delta e = 0.05$, and $\Delta I = 2°$ of Eros' osculating orbit ($a_{\rm Eros} = 1.458$ AU, $e_{\rm Eros} = 0.223$, and $I_{\rm Eros} = 10.829°$).

Our test body integration tracks yielded several positive matches with this criteria. We found that 10 of the 3300 test bodies started in the ν_6 resonance reached Eros' orbit, while 2 of 987 test bodies started in the 3:1 resonance did the same (see Bottke et al., 2002, for definitions). For the diffusive resonances, we found that 755 of the bodies started in the intermediate Mars-crossing region adjacent to the main belt with $a < 2.5$ AU reached NEA orbits (perihelion $q < 1.3$ AU) and 4 of that sample reached an Eros-like orbit. When coupled from results from Bottke et al. (2002), who show that 37, 25, and 23% of all NEAs come from ν_6 resonance, the intermediate source Mars-crossers (IMC) region, and the 3:1 resonances, respectively, we predict that NEAs originating in the inner main belt has a 0.35% probability of achieving an Eros-like orbit.

Figure 9 shows an example of our results (in Table 1, this orbit is called `orb.imc.1`). This orbit initially resides in the intermediate Mars-crossing zone, though it is also affected by the ν_6 secular resonance as readily seen from the left and bottom part of Fig. 9. Mars-encounters drive the orbit to encounter the Earth at $\simeq$4 Myr, which makes this orbit drift more deeply into the planet-crossing region. Note the proper inclination computed with our method still represents the osculating inclination evolution. At time $\simeq$13.18 Myr, the osculating orbit approaches the current orbital elements of Eros ($a = 1.47$ AU, $e = 0.28$, and $I = 10.91°$). Interestingly, we note that our test body becomes decoupled from Earth's orbit slightly before acquiring these a, e, I values.

4.2. Eros' spin evolution coupled to its orbital evolution

Using our sample of potential Eros orbital histories (Table 1), we investigated whether Eros' current spin state, namely the residence of its pole in the s-resonance, is somehow linked to its orbital evolution. Our method is similar to that used in Section 3.1; we will use our orbital his-

Table 1
Statistics of meeting the constraints provided by Eros' current spin state

Orbit	p_1	p_2	p_3	p_4	T	f	$I_{\max}$
IMC orbits[a]							
`orb.imc.1`[b]	11.8	16.1	15.3	8.8	13.18	0.663	20.8
`orb.imc.2`	13.4	13.8	13.6	12.1	99.04	0.070	37.4
`orb.imc.3`	1.4	2.6	2.3	0.8	68.88	0.024	12.5
`orb.imc.4`[c]	17.1	23.3	19.3	15.6	84.16	0.026	23.8
ν_6 orbits[a]							
`orb.nu6.1`	12.7	16.5	23.9	3.9	9.42	0.276	20.5
`orb.nu6.2`	13.3	20.0	23.2	5.1	6.27	0.457	14.3
`orb.nu6.3`	12.6	15.5	16.7	4.8	23.38	0.749	20.6
`orb.nu6.4`	12.5	13.2	17.7	5.9	46.18	0.304	25.3
`orb.nu6.5`[c]	16.2	22.3	30.2	5.9	20.47	0.077	16.9
`orb.nu6.6`	9.2	13.6	9.7	8.0	38.39	0.022	30.1
`orb.nu6.7`[c]	16.1	17.7	27.4	7.2	21.68	0.265	27.8
`orb.nu6.8`	14.2	15.5	18.1	10.1	23.30	0.424	26.6
`orb.nu6.9`	3.4	3.3	3.4	2.4	18.65	0.522	24.9
`orb.nu6.10`	9.8	14.9	14.0	5.4	2.80	0.747	18.4
3/1 orbits[a]							
`orb.3/1.1`	16.2	16.6	20.5	13.2	178.77	0.195	31.6
`orb.3/1.2`	11.6	14.9	12.6	9.2	8.23	0.684	31.9

[a] Source regions for the orbital evolution; see Bottke et al. (2002) for definitions and details.
[b] The orbit shown in Figs. 9 and 10.
[c] These orbits give the most satisfactory results.
The libration in the s-resonance with amplitude $\leqslant 160°$ was determined using a numerical model that assumes (i) uniform initial data in $(\cos\varepsilon_0, \psi_0)$ and (ii) spin propagation along all orbits that reach Eros orbital cell in semi-major axis, eccentricity and inclination space (see Section 4.2). The values p_1–p_4 are the probabilities that our model asteroid will match Eros' spin state from different subsets of the initial data: (i) p_1 is the overall probability, (ii) p_2 is the probability for initially prograde rotation states only, (iii) p_3 is the probability for the initial states with $|\cos\varepsilon_0| \leqslant 0.25$ (i.e., initial spin orientation preferentially in the orbital plane), and (iv) p_4 is the probability for those initial states with $|\cos\varepsilon_0| \geqslant 0.75$ (i.e., initial spin orientation preferentially perpendicular to the orbital plane). The last three columns are: (i) T is the time needed for our main belt test bodies to match Eros' a, e, I orbital parameters (in Myr), (ii) f is the fraction of that time interval spent on an Earth-crossing orbit, and (iii) $I_{\max}$ is the maximum inclination acquired during the evolution.

tories as input to compute the functions $\mathcal{A}, \mathcal{B}, \mathcal{C}$, and α and integrate Eqs. (7)–(8), assuming that[6] $\bar{\mathbf{T}} = 0$ (thus ω is constant). Unlike our predictions of Eros' future evolution, however, Eros' initial conditions are unknown. To deal with this problem, we use a broad set of initial data that is spatially isotropic: $\cos\varepsilon_0 = -0.975, \ldots, 0.975$ with an increment 0.025 and $\psi_0 = 0°, \ldots, 360°$ with an increment 5°. Together, this means that for every one of Eros' orbital pathways, we need to run 5688 spin evolution simulations. In each simulation, we monitored whether our model asteroid, when reaching an orbital match with Eros, would also have its spin pole locked in the s-resonance over a 0.5 Myr window. We considered a positive match to be a pole solution that librates within 160° of the resonance angle φ.

To illustrate how Eros' orbital evolution may have affected its spin evolution, consider the example case using the `orb.imc.1` orbit from Section 4.1. Using the uniform grid of data described above, we found that Eros' pole was trapped in the s-resonance $\simeq$11.8% of the time (672 runs out of 5688). The probability of matching Eros' pole using a more select sample of initial data, such as the initially-prograde rotation states only, are given in the Table 1.

The spin state evolution of our model asteroid for one of our successful matches is shown in Fig. 10. In this case, we purposely chose initial conditions that are very different from current Eros values ($\varepsilon_0 = 12.838°$ and $\psi_0 = 25°$) to illustrate that there may be zero connection between our initial and final parameters. The figure shows that the chaotic, irregular evolution of Eros' orbit causes Eros' pole to bounce between various resonant states. In particular, Fig. 10 shows that Eros' pole is immediately captured in the s-resonance,[7] with the obliquity oscillating in between 15° and 65°. It drops out, however, when large e variations produced by Eros' orbital interaction with the ν_6 secular resonance reduces κ and virtually eliminates the spin–orbit resonance altogether. Overall, we find that Eros' pole is captured by the s-resonance several times during the simulation, with one capture occurring just when our model asteroid matched Eros' orbital constraints at $\simeq$13 Myr.

To understand why Eros' pole has such a low chance being captured by the s-resonance, we plotted the distribution of a 0.5 Myr-averaged final obliquity values $\bar{\varepsilon}$ for the `orb.imc.1` orbit from all 5688 simulations (Fig. 11). The most striking feature is the strong peak at $\cos\bar{\varepsilon} \simeq 0.139$ that corresponds to Cassini state 2. This suggests that even though the likelihood of attaining this resonant state versus the *cumulative* probability of all possibilities is relatively small, we are more likely to find Eros' pole in the s-resonance than any other individual possibility. We also checked to see if Eros' evolution would have led to an overabundance of poles in the resonance. Using a method described by Henrard and Murigande (1987), we estimated that an isotropic distribution of pole directions would lead to $\simeq$21% being inside the resonance zone about the Cassini state 2. Given the similarity between this value and those in Table 1 (in particular the probability value p_1 that corresponds to the initially isotropic spin data), it appears in this case that Eros' orbital evolution does not push its pole towards a resonant state. Recall that in our model Eros spin axis can only be affected by gravitational and inertial torques.

To determine whether this result is applicable to all possible orbital histories of Eros, we used this same method to

[6] The current best estimates of the Yarkovsky and, especially, the YORP effects acting on Eros (e.g., Vokrouhlický, 1998; Vokrouhlický and Čapek, 2002; Čapek and Vokrouhlický, 2004) indicate those forces should play a minimal role over timescales shorter than $\simeq$100 Myr. For this reason, we concentrate here on solar and planetary gravitational forces alone.

[7] Our experience shows that prograde-rotating asteroids in the inner part of the main asteroids belt become typically captured by this resonance; e.g., Rubincam et al. (2002) pointed out that the Asteroid (951) Gaspra spin axis currently resides in this resonance.

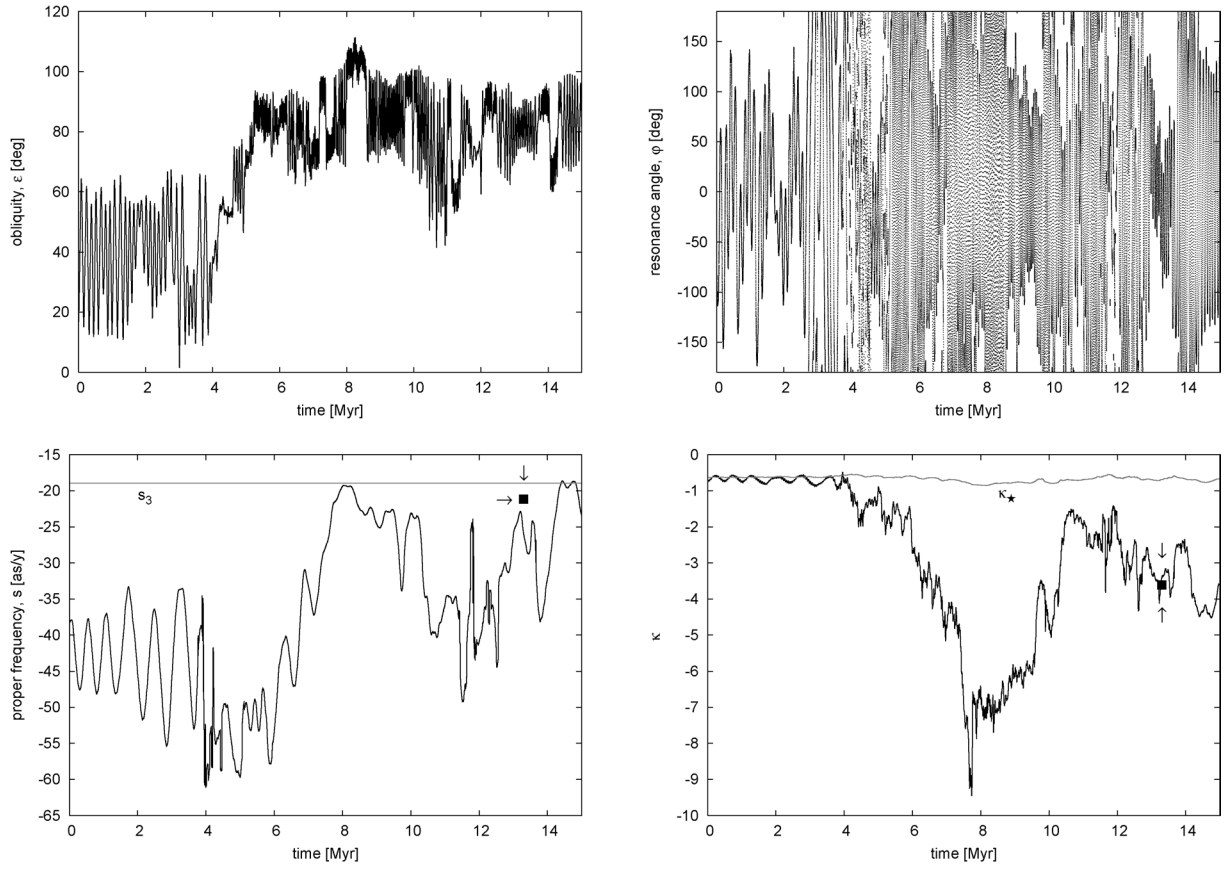

Fig. 10. An example of a possible spin evolution for a "fake Eros" evolving from the inner main belt along the orbit shown in Fig. 9. The initial value of the obliquity and the precession in longitude were $\varepsilon_0 = 12.84°$ and $\psi_0 = 25°$. The four panels show the time dependence of: obliquity ε (left and top), the critical angle φ of the s spin–orbit resonance (right and top), the proper frequency s in ξ (left and bottom), and the κ factor (right and bottom). The last panel also shows the critical value $\kappa_\star$ (in gray) for which the secular spin–orbit resonance bifurcates. The current Eros value of s and κ are shown in the last two panels; they were drawn at time $\simeq$13.18 Myr when the clone's a, e, I parameters closely matched Eros' current values. Initially, the spin–orbit resonance is only marginally possible ($\kappa \leqslant \kappa_\star$) due to large cycles in e driven by the ν_6 orbital resonance. The evolution of Eros' orbit into the planet-crossing region makes κ smaller but planetary perturbations prevent Eros from being confined in a resonance for very long. Near $\simeq$13.18 Myr, the spin–orbit resonance is re-gained, and both the orbit and the spin location end up matching Eros' current parameters.

track Eros' spin evolution over several additional histories comparable to `orb.imc.1`. Our results are summarized in Table 1. Overall, we found no trends other than a weak asymmetry that suggested that asteroids with initially prograde sense of rotation were more likely to produce resonant spin states than those with retrograde sense of rotation. This is likely due to the fact that obliquities between 0°–90° are efficiently mixed by chaotic diffusion due to a network of secular spin–orbit resonances. We also note that many of our successful matches were of shorter duration and larger amplitude in resonance angle than found in Section 3.1 for our future Eros test cases.

Except for the feature related to the spin–orbit resonance, the distribution shown in the Fig. 11 is surprisingly uniform (see also Skoglöv, 1999). We believe this arises from (i) the strong chaoticity and mixing of spin states in Eros' evolution and (ii) the fact that the apparent asymmetry in the prograde vs. retrograde rotation states due to presence of secular resonances in the prograde-rotators zone only does not operate. With (ii), one might expect the initially prograde spin states to be more easily driven to final retrograde states. However, lightcurves taken from Fig. 11 show that while the initial prograde spins populate the final retrograde ones, the same fraction of initially retrograde spins populate the final prograde ones. This produces an effective cancellation and makes the final distribution statistically equivalent to a uniform distribution. We hypothesize that the powerful s-resonance zone near 90° obliquity is responsible for this communication between prograde and retrograde states. Confirming this would require a more extensive and systematic study and is beyond the scope of this paper.

5. Discussion and conclusions

Our results in Section 4.2 suggest that Eros' current spin–orbit resonant state is something of a fluke, with Eros' past orbital evolution neither helping or hurting its ability to reach that state. The IMC and ν_6 zones seem slightly more likely to produce the current Eros spin state, though we are limited here by poor statistics. Although we cannot rule out the

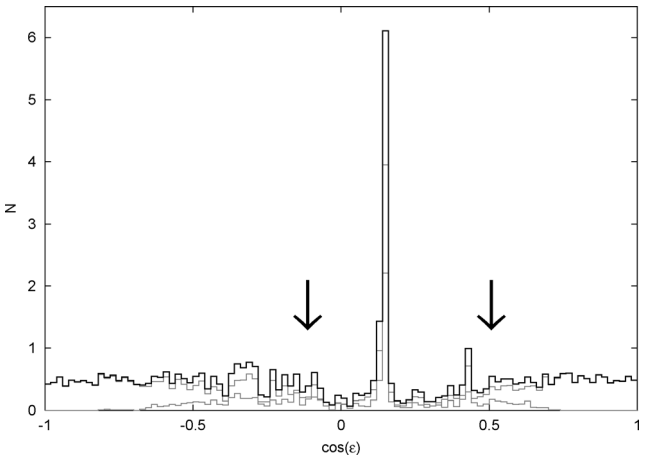

Fig. 11. Statistical distribution of $\cos\bar{\varepsilon}$, where $\bar{\varepsilon}$ is the mean obliquity between 13–13.5 Myr computed from the numerical propagation of 5688 test runs along the orbit `orb.imc.1` from Fig. 9. The overall distribution is given as a thick black line, while distributions from initially prograde/retrograde are shown as thin gray lines. The initial data corresponds to an *isotropic* spin distribution, thus the distribution function =0.5 for the normalization used here. The singular peak at $\cos\bar{\varepsilon} \simeq 0.139$ shows states trapped in the s-resonance (arrows delimit the maximum width of the resonance in obliquity). Being located in the resonance is the most likely state among all the bins. The probability of being in the resonance, however, is only ≃14% of the total probability over all other bins. The retrograde states are roughly as likely as the prograde ones (excluding the resonance peak), even though there is considerable mixing between the prograde and retrograde orbits (see the "overshoots" beyond the 90° obliquity of the thin lines).

possibility that this is the true answer, we suspect that our model might be missing some important piece of the puzzle. To this end, we postulate that a dissipative mechanism acting on Eros rotation over the long term may increase the odds that Eros would be in a spin–orbit resonance today.

One possibility is that Eros' spin state has been affected by distant tidal forces. The Moon is an example of an object that has reached Cassini state 2 (or 1 when the state 2 does not exist) via anelastic tidal processes (e.g., Ward, 1975; Peale, 1977; Gladman et al., 1996). The same can be said for Mercury (e.g., Ward, 1975; Peale, 1974, 1988) and, in a generalized way, Venus (e.g., Ward, 1975; Ward and De Campli, 1979; Dobrovolskis, 1980; Correia and Laskar, 2001; Correia et al., 2003).

In order to estimate the role of tidal effects on Eros spin state, we use the Darwin–Mignard model (Mignard, 1979). To keep our model simple, we assume that tidal torque for a body on circular orbit about the Sun; this approximation does not effect our results unless Eros' $e > 0.6$. Using the notation from Section 2, we have:

$$\bar{\mathbf{T}} = -n^2 C\beta\left(\mathbf{e} + \mathbf{n}\cos\varepsilon - 2\frac{n}{\omega}\mathbf{n}\right) + \mathcal{O}(e^2), \tag{27}$$

where we introduced a nondimensional, tidal-strength factor

$$\beta = \frac{3}{2}\left(\frac{R_a}{a}\right)^5 \frac{Ma^2}{C}\frac{k_2\delta}{1-n/\omega}. \tag{28}$$

Here, R_a is the characteristic radius of the asteroid, M is the solar mass, k_2 is the quadrupole Love number and $\delta = (\omega - n)\Delta t$ is the phase lag of tidal response due to anelasticity. For Eros, we estimate that $\beta \simeq 2.5\times10^{-8}k_2\delta$. With k_2 of the order of unity (this value is likely too high because Eros has a nonzero rigidity) and $\delta \simeq 10^{-2}$, we obtain $\beta \simeq 2.5\times10^{-10}$.

Inserting (27) into Eqs. (6)–(8), we obtain tidal components that affect the evolution Eros' rotation rate ω and obliquity ε (e.g., also Dobrovolskis, 1980; Correia et al., 2003; eccentricity terms $\mathcal{O}(e^2)$ again omitted):

$$\left(\frac{d\omega}{dt}\right)_T = -n^2\beta\left(1+\cos^2\varepsilon - 2\frac{n}{\omega}\cos\varepsilon\right), \tag{29}$$

$$\left(\frac{d\varepsilon}{dt}\right)_T = n\beta\frac{n}{\omega}\sin\varepsilon\left(\cos\varepsilon - 2\frac{n}{\omega}\right), \tag{30}$$

$$\left(\frac{d\psi}{dt}\right)_T = 0. \tag{31}$$

The timescale needed to produce a sizeable change in spin parameters from tides is $\tau \simeq \omega/(n^2\beta) \simeq 10^4$ Gyr. This value is far too long to have any importance on Eros' history.

A second possibility is that Eros' spin pole was affected in the recent past by a close planetary encounter (Bottke et al., 1999). Results from Richardson et al. (1998) suggest that significant changes to Eros' obliquity can occur during such encounters if Eros also experiences mass loss via tidal disruption. The damage produced by such an event would include global landslides that would modify, bury, or erase existing craters. Because images of Eros from NEAR/Shoemaker fail to show evidence for such a large-scale crater erasure event, we believe that close encounters have not seriously affected Eros' spin pole over its lifetime.

Finally, it is plausible that Eros' has been affected by a dissipative torque produced by radiative and thermal recoil effects collectively known as the YORP effect (Rubincam, 2000; Vokrouhlický and Čapek, 2002; Bottke et al., 2003). Rubincam (2000) and Vokrouhlický and Čapek (2002) computed that YORP torques should drive Eros' obliquity towards 90°, provided the surface thermal conductivity is $K \sim 0$ W/(m K). They also found that the typical timescale to significantly affect the obliquity by the YORP effect is ≃500–700 Myr. If Eros had a 90° obliquity before it left the main belt, it would have a much larger probability of residing in a spin–orbit resonance today (see probability values p_3 in the Table 1). Čapek and Vokrouhlický (2004), on the other hand, found that for values $K \geqslant 5\times10^{-4}$ W/(m K) the asymptotic YORP obliquity becomes 0° or 180° and near that threshold value of the surface conductivity the obliquity evolves on a timescale about an order of magnitude longer than with $K \sim 0$ W/(m K). Though there is considerable uncertainty about K values for all asteroids, it is believed that $K \simeq 0.001$ W/(m K) are common among Eros-sized main belt asteroids. The infrared observations by Morrison (1976), while providing an indirect measure only, indicate a slightly higher value of the thermal conductivity. Still, if

Eros is several Gyr old, as is suggested by its heavily cratered surface (e.g., Chapman, 2003), even weak YORP torques would have time to substantially affect its obliquity. Note that Eros is actually smaller than many of the Koronis family asteroids that are known to be in spin–orbit resonances (e.g., Vokrouhlický et al., 2003). We believe an exploration of Eros' spin state evolution in the main belt is the next logical step in our work, with a reliable Eros-YORP model a prerequisite to obtaining the best possible results.

Acknowledgments

The work of David Vokrouhlický has been supported by the Grant Agency of the Czech Republic. William Bottke's research on this project was supported by NASA's Planetary Geology and Geophysics program (Grant NAG513195) and NASA's Discovery Data Analysis Program (Grant NNG04GA75G). Both D.V. and W.B. also thank the support they received from the National Science Foundation's COBASE travel grant program. David Nesvorný's research on this project was supported by NASA's Planetary Geology and Geophysics Program (Grant PGG02-0106-0111). We thank E. Skoglöv who, as a referee, helped to improve the final version of this text. This paper profited from several discussions with A.W. Harris (SSI).

References

Berberich, A., 1898. Erste Bahnbestimmung des Planeten 1898 DQ. Astron. Nachr. 147, 221–224.

Bertotti, B., Farinella, P., Vokrouhlický, D., 2003. Physics of the Solar System. Kluwer Academic, Dordrecht.

Bottke, W.F., 2001. On the orbital and collisional history of (433) Eros. In: AGU Fall Meeting 2001. Abstract P32B-0557.

Bottke, W.F., Richardson, D.C., Michel, P., Love, S.G., 1999. 1620 Geographos and 433 Eros: shaped by planetary tides? Astron. J. 117, 1921–1928.

Bottke, W.F., Jedicke, R., Morbidelli, A., Petit, J.-M., Gladman, B., 2000. Understanding the distribution of near-Earth asteroids. Science 288, 2190–2194.

Bottke, W.F., Vokrouhlický, D., Brož, M., Nesvorný, D., Morbidelli, A., 2001. Dynamical spreading of asteroid families via the Yarkovsky effect: the Koronis family and beyond. Science 294, 1693–1696.

Bottke, W.F., Morbidelli, A., Jedicke, R., Petit, J.-M., Levison, H.F., Michel, P., Metcalfe, T.S., 2002. Debiased orbital and absolute magnitude distribution of the near-Earth objects. Icarus 156, 399–433.

Bottke, W.F., Vokrouhlický, D., Rubincam, D.P., Brož, M., 2003. Dynamical evolution of asteroids and meteoroids using the Yarkovsky effect. In: Bottke, W.F., Cellino, A., Paolicchi, P., Binzel, R.P. (Eds.), Asteroids III. Univ. of Arizona Press, Tucson, pp. 395–408.

Čapek, D., Vokrouhlický, D., 2004. The YORP effect with finite thermal conductivity. Icarus 172, 526–536.

Chandler, S.C., 1898. The small planet 1898 DQ 1 (433) Eros at the oppositions of 1893–94 and 1896. Astron. J. 19, 160–162.

Chapman, C.R., 2003. Cratering on asteroids from Galileo and NEAR Shoemaker. In: Bottke, W.F., Cellino, A., Paolicchi, P., Binzel, R.P. (Eds.), Asteroids III. Univ. of Arizona Press, Tucson, pp. 315–430.

Chapman, C.R., Merline, W.J., Thomas, P.C., Joseph, J., Cheng, A.F., Izenberg, N., 2002. Impact history of Eros: craters and boulders. Icarus 155, 104–118.

Cheng, A., 2003. Near Earth asteroid rendezvous: mission summary. In: Bottke, W.F., Cellino, A., Paolicchi, P., Binzel, R.P. (Eds.), Asteroids III. Univ. of Arizona Press, Tucson, pp. 351–366.

Colombo, G., 1966. Cassini's second and third laws. Astron. J. 71, 891–896.

Correia, A.C.M., Laskar, J., 2001. The four final rotation states of Venus. Nature 411, 767–770.

Correia, A.C.M., Laskar, J., Néron de Surgy, O., 2003. Long-term evolution of the spin of Venus. I. Theory. Icarus 163, 1–23.

Crommelin, A.C.D., 1898. The new planet DQ. The Observatory 21, 370–375.

Dobrovolskis, A.R., 1980. Atmospheric tides and the rotation of Venus. II. Spin evolution. Icarus 41, 18–35.

Ferraz-Mello, S., 1981. Estimation of periods from unequally spaced observations. Astron. J. 86, 619–624.

Froeschlé, Ch., Hahn, G., Gonczi, R., Morbidelli, A., Farinella, P., 1995. Secular resonances and the dynamics of Mars-crossing and near-Earth asteroids. Icarus 117, 45–61.

Gladman, B., Quinn, D.D., Nicholson, P., Rand, R., 1996. Synchronous locking of tidally evolving satellites. Icarus 122, 166–192.

Greenberg, R., Bottke, W.F., Michael, M., Geissler, P., Petit, J.-M., Durda, D.D., Asphaug, E., Head, J., 1996. Collisional and dynamical history of 243 Ida. Icarus 120, 106–118.

Gronchi, G.F., Milani, A., 2001. Proper elements for Earth-crossing asteroids. Icarus 152, 58–69.

Henrard, J., Murigande, C., 1987. Colombo's top. Celest. Mech. 40, 345–366.

Hinks, A.R., 1904. Sun, parallax of the, from photographs of Eros. Mon. Not. R. Astron. Soc. 64, 701–727.

Innes, R.T.A., 1931. The shape of Eros in 1924. Astron. Nachr. 241, 55.

Konopliv, A.S., Miller, J.K., Owen, W.M., Yeomans, D.K., Giorgini, J.D., Garmier, R., Barriot, J.-P., 2002. A global solution for the gravity field, rotation, landmarks and ephemeris of Eros. Icarus 160, 289–299.

Krug, W., Schrutka-Rechtenstamm, G., 1937. Untersuchungen über Gestalt und Größe des Planetoiden Eros. Z. Astrophys. 13, 1–12.

Laskar, J., Robutel, P., 1993. The chaotic obliquity of the planets. Nature 361, 608–612.

Levison, H., Duncan, M., 1994. The long-term dynamical behavior of short-period comets. Icarus 108, 18–36.

Lieske, J.H., 1968. Mass of the Earth–Moon system from observations of Eros, 1893–1966. Astron. J. 73, 628–643.

Marzari, F., Davis, D., Vanzani, V., 1995. Collisional evolution of asteroid families. Icarus 113, 168–187.

Michel, P., 1997. Effects of linear secular resonances in the region of semimajor axes smaller than 2 AU. Icarus 129, 348–366.

Michel, P., Froeschlé, Ch., 1997. The location of linear secular resonances for semimajor axes smaller than 2 AU. Icarus 128, 230–240.

Michel, P., Thomas, F., 1996. The Kozai resonance for near-Earth asteroids with semimajor axes smaller than 2 AU. Astron. Astrophys. 307, 310–318.

Michel, P., Farinella, P., Froeschlé, Ch., 1998. Dynamics of Eros. Astron. J. 116, 2023–2031.

Mignard, F., 1979. The evolution of the lunar orbit revisited. Moon Planets 20, 301–315.

Milani, A., Carpino, M., Hahn, G., Nobili, A.M., 1989. Dynamis of planet-crossing asteroids: classes of orbital behaviour. Icarus 78, 212–269.

Miller, J.K., 10 colleagues, 2002. Determination of shape, gravity, and rotational state of Asteroid 433 Eros. Icarus 155, 3–17.

Morbidelli, A., 2002. Modern Celestial Mechanics: Aspects of Solar System Dynamics. Taylor & Francis, London.

Morrison, D., 1976. The diameter and thermal inertia of 433 Eros. Icarus 28, 125–132.

Néron de Surgy, O., Laskar, J., 1997. On the long term evolution of the spin of the Earth. Astron. Astrophys. 318, 975–989.

Newcomb, S., 1898. Usefulness of the planet DQ for determining the solar parallax. Astron. J. 20, 147–148.

von Oppolzer, E., 1901. Vorläufige Mittheilung über photometrische Messungen des Planeten (433) Eros. Astron. Nachr. 154, 309–312.

Peale, S.J., 1969. Generalized Cassini's laws. Astron. J. 74, 483–489.
Peale, S.J., 1974. Possible histories of the obliquity of Mercury. Astron. J. 79, 722–744.
Peale, S.J., 1977. Rotation histories of the natural satellites. In: Burns, J.A. (Ed.), Planetary Satellites. Univ. of Arizona Press, Tucson, pp. 87–111.
Peale, S.J., 1988. The rotational dynamics of Mercury and the state of its core. In: Vilas, F., Chapman, C.R., Matthews, M.S. (Eds.), Mercury. Univ. of Arizona Press, Tucson, pp. 461–493.
Pickering, E.C., 1905. Early observations of Eros (433). Ann. Harvard College Observatory 53, 187–230.
Rabe, E., 1950. Derivation of fundamental astronomical constants from the observations of Eros during 1926–1945. Astron. J. 55, 112–125.
Rabe, E., Francis, M.P., 1967. The Earth + Moon mass and other astronomical constants from the Eros motion 1926–1965. Astron. J. 72, 856–864.
Richardson, D.C., Bottke, W.F., Love, S.G., 1998. Tidal distortion and disruption of Earth-crossing asteroids. Icarus 134, 47–76.
Rubincam, D.P., 2000. Radiative spin-up and spin-down of small asteroids. Icarus 148, 2–11.
Rubincam, D.P., Rowlands, D.D., Ray, R.D., 2002. Is Asteroid 951 Gaspra in a resonant obliquity state with its spin increasing due to YORP? J. Geophys. Res. 107 (E9), 5065.
Scheeres, D.J., Ostro, S.J., Werner, R.A., Asphaug, E., Hudson, R.S., 2000. Effects of gravitational interactions on asteroid spin states. Icarus 147, 106–118.
Skoglöv, E., 1997. Evolution of the obliquities for nine near-Earth asteroids. Planet. Space Sci. 45, 439–447.
Skoglöv, E., 1999. Spin vector evolution for inner Solar System asteroids. Planet. Space Sci. 47, 11–22.
Slivan, S.M., 2002. Spin vector alignment of Koronis family asteroids. Nature 419, 49–51.
Slivan, S.M., Binzel, R.P., Crespo da Silva, L.D., Kaasalainen, M., Lyndaker, M.M., Krčo, M., 2003. Spin vectors in the Koronis family: comprehensive results from two independent analyses of 213 rotation lightcurves. Icarus 162, 285–307.
Souchay, J., Kinoshita, H., Nakai, H., Roux, S., 2003. A precise modeling of Eros 433 rotation. Icarus 166, 285–296.
Veverka, J., 32 colleagues, 2000. NEAR at Eros: imaging and spectral results. Science 289, 2088–2097.
Vokrouhlický, D., 1998. Diurnal Yarkovsky effect for meter-sized asteroidal fragments' mobility. I. Linear theory. Astron. Astrophys. 335, 1093–1100.
Vokrouhlický, D., Čapek, D., 2002. YORP-induced long-term evolution of the spin state of small asteroids and meteoroids. Rubincam's approximation. Icarus 159, 449–467.
Vokrouhlický, D., Nesvorný, D., Bottke, W.F., 2003. The vector alignments of asteroid spins by thermal torques. Nature 425, 147–152.
Ward, W.R., 1974. Climatic variations on Mars. Astronomical theory of insolation. J. Geophys. Res. 79, 3375–3386.
Ward, W.R., 1975. Tidal friction and generalized Cassini's laws in the Solar System. Astron. J. 80, 64–70.
Ward, W.R., De Campli, W.M., 1979. Comments on the Venus rotation pole. Astrophys. J. 230, L117–L121.
Witt, G., 1898. Entdeckung eines neuen Planeten 1898 DQ. Astron. Nachr. 147, 141.
Yeomans, D.K., 15 colleagues, 2000. Radio science results during the NEAR-Shoemaker spacecraft rendezvous with Eros. Science 289, 2085–2088.